Cardiac muscle *in vitro* is more energetically efficient contracting against an *in silico* model of the hemodynamic impedance of the arterial system

Amy S. Garrett[1*], Denis S. Loiselle[1,2], Andrew J. Taberner[1,3], June-Chiew Han[1]

[1] Auckland Bioengineering Institute, The University of Auckland, New Zealand

[2] Department of Physiology, The University of Auckland, New Zealand

[3] Department of Engineering Science, The University of Auckland, New Zealand

Running Title: Energetics of Windkessel-loaded cardiac muscle

Key words: Cardiac muscle, Work-loop, Efficiency, Mechano-energetics, Windkessel

* Correspondence:

Amy Garrett

ORCID: 0000-0002-7176-0918

Auckland Bioengineering Institute

70 Symonds Street, Auckland, New Zealand

amy.garrett@auckland.ac.nz

First Author Profile

Dr Amy Garrett completed her Masters of Bioengineering in 2017 and her PhD in Bioengineering in 2021, both from the Auckland Bioengineering Institute at The University of Auckland, New Zealand. Her PhD research expanded her ME project and focused on developing various model-based approaches to understanding isolated cardiac muscle mechano-energetics. Developed models include real-time presentation of preload and afterload for novel work-loop contraction protocols implemented in a calorimeter device. Amy has recently embarked on a postdoc research project, at the Auckland Bioengineering Institute, where she is developing measurement techniques for uterine smooth muscle electrophysiology.

Key Points Summary

- We assessed the energetic consequence of contraction of cardiac muscle samples *in vitro* experiencing the *in vivo* hemodynamic impedance of the arterial system.

- We compared it to that measured with a conventional experimental method where muscle shortening during contraction is constrained to remain at a constant force and is arbitrarily defined.

- Our impedance-loading method does not constrain the dynamics of muscle shortening and, hence, allows muscles to describe their natural shortening dynamics while performing force-length work and liberating heat.

- We found that impedance-loaded cardiac muscles shortened more slowly and produced greater work output, and force, than during conventional shortening. These obtained with negligible changes in the extent of shortening and heat production, thereby yielding greater mechanical efficiency.

- This study reveals that differences in the shortening kinetics of the cardiac cycle can impact muscle efficiency in performing mechanical work.

Abstract

Conventional experimental methods for studying cardiac muscle *in vitro* often do not expose the tissue preparations to a mechanical impedance that resembles the *in vivo* hemodynamic impedance dictated by the arterial system. That is, the afterload in work-loop contraction is conventionally simplified to be constant throughout muscle shortening, and at a magnitude arbitrarily defined. This conventional afterload does not capture the time-varying interaction between the left ventricle and the arterial system. We have developed a contraction protocol for isolated tissue experiments that allows the afterload to be described within a Windkessel framework that captures the mechanics of the large arteries and peripheral arterial resistance. We compared energy expenditure of isolated rat left-ventricular trabeculae undergoing the two different protocols of force-length work-loop contractions: conventional versus Windkessel loading. Mechanical work and heat liberation were assessed, and mechanical efficiency quantified. We found that both extent of shortening and heat output were unchanged between protocols, but peak shortening velocity was 39.0 % lower and peak work output was 21.8 % greater when muscles contracted against the Windkessel afterload than against the conventional isotonic afterload. The greater work led to a 25.2 % greater mechanical efficiency. Our findings highlight that the mechanoenergetic performance of cardiac muscles *in vitro* may have been constrained by the conventional, arbitrary, loading method. A Windkessel loading protocol, by contrast, unleashes more cardiac muscle mechanoenergetic potential and allows improved investigation of the effects of arterial hemodynamics.

Introduction

Beat-by-beat ventricular contraction is characterised by pressure-volume loops consisting of four sequential phases: isovolumic contraction, after-loaded ejection, isovolumic relaxation and diastolic refilling. The ejection phase, including its transition from and to its adjacent phases, is of particular interest as its mechanics are closely coupled to the dynamics of the arterial system. The resistance and compliance of the large arteries, and the downstream impedance of the peripheral arterial systems, affect the extent and timing of pressure developed by the ventricles. The energy stored during systole in the large elastic arteries is then dissipated by the blood throughout the arterial system during diastole This coupling between the ventricle and the arterial system was first described by Frank (Frank, 1899) (translated into English (Sagawa *et al.*, 1990)) with the use of a 2-element Windkessel model comprising an arterial compliance (C) and a peripheral resistance (R_P). This 2-element model was later expanded to include a third element in order to capture the characteristic aortic impedance (Z_C) (Westerhof *et al.*, 1969; Westerhof *et al.*, 2009). The 3-element Windkessel model has since formed part of experimental or analytical protocols for the study of left-ventricular (Elzinga & Westerhof, 1973; Suga & Sagawa, 1977; Elzinga & Westerhof, 1980; Sunagawa *et al.*, 1982; Sunagawa *et al.*, 1983; Maughan *et al.*, 1984; Sunagawa *et al.*, 1985; Midei *et al.*, 1987; De Tombe *et al.*, 1993) and right-ventricular (Lankhaar *et al.*, 2006; Saouti *et al.*, 2010; Chemla *et al.*, 2015; Fukumitsu *et al.*, 2016) physiology in healthy and diseased (Sunagawa *et al.*, 1983; Fukumitsu *et al.*, 2016) whole-hearts.

When studying isolated muscle samples using trabeculae (Goo *et al.*, 2009; Han *et al.*, 2010; Taberner *et al.*, 2010; Taberner *et al.*, 2011a), papillary muscles (Hisano & Cooper, 1987; Layland *et al.*, 1995; Sorhus *et al.*, 2000; Mellors & Barclay, 2001; Mellors *et al.*, 2001; Barclay *et al.*, 2003) or individual cardiomyocytes (Iribe *et al.*, 2007; Iribe *et al.*, 2014; Helmes *et al.*, 2016), the force-length work-loops also consist of four sequential phases to resemble the pressure-volume loop *in vivo*: isometric contraction, afterloaded shortening, isometric relaxation and diastolic re-lengthening. The conventional method to achieve force-length work-loops involves controlling muscle length during the afterloaded shortening phase in order to maintain a constant value of force, arbitrarily chosen by the experimentalist. This simplified method results in ‘flat-topped’ force-length work-loops. These loops do not fully reflect the dynamic, time-varying, nature of the ejection phase that is modulated by ventricular-arterial coupling *in vivo*, typically exemplified by the dynamic, curved nature of the ejection trajectory of the pressure-volume loop. Crucially, a trabecula that is constrained to follow a ‘flat-topped’ shortening trajectory may not fully realise its potential to produce mechanical work, nor operate at its maximum energetic efficiency.

Loading protocols using 3-element Windkessel impedance loads have been adopted in isolated tissue experiments, using pre-calculated loads, to evaluate cardiac muscle mechanics (Elzinga & Westerhof, 1981, 1982; de Tombe & Little, 1994). The current study extends the use of 3-element Windkessel impedance loads in isolated tissue experiments to encompass energetics by determining muscle energy efficiency from the ratio of work to the sum of work and active heat. Our model-based loading protocol incorporates a 3-element Windkessel model of vascular impedance (Garrett *et al.*, 2017; Garrett *et al.*, 2019). This impedance, computed in real-time, rather than pre-calculated, gives rise to force-length shortening profiles that better mimic the dynamic pressure-volume ejection profiles. This study compares cardiac mechano-energetic performance of isolated trabeculae between that which arises when contracting against a 3-element Windkessel model with that which arises when they are subjected

112 to perform the conventional ‘flat-topped’ work-loops. Muscle mechano-energetic performance was
113 assessed over a wide range of loads by varying the model parameter governing the arterial peripheral
114 resistance.

Methods

The Work-Loop calorimeter

Experiments were conducted using a work-loop calorimeter (Taberner *et al.*, 2005; Han *et al.*, 2009; Taberner *et al.*, 2011a, b). This device consists of a borosilicate glass measurement chamber (internal dimensions 1 mm square) inserted in a block of thermally conductive gold-plated copper. In each experiment, a trabecula was suspended between two platinum hooks in the measurement chamber and supplied with a constant flow of oxygen- and nutrient-rich Tyrode superfusate. Thermopile sensors mounted below and external to the measurement chamber generated a voltage proportional to the temperature increase of the superfusate as it flowed over the trabecula. The increased temperature of the superfusate was proportional to the rate of heat-release by the muscle.

A linear voice-coil motor, connected to the upstream hook, controlled muscle length. Muscle force development was measured using a cantilever-based force transducer connected to the downstream hook. Bending of the cantilever and the position of the linear motor were measured by a laser interferometer system. A LabVIEW RealTime and field-programmable gate array (FPGA) system houses the control architecture, which enables the performance of a range of contraction modes including isometric contractions (no shortening), and two shortening contractions: conventional constant-afterload ('flat-top') work-loops and Windkessel-loaded work-loops.

Conventional versus Windkessel work-loop loading

Isometric contractions, where muscle length was controlled to remain unchanged throughout a twitch, were achieved by compensating for the tiny deflection of the force transducer downstream with the upstream length-motor. In the conventional flat-top work-loop control mode, on elicitation of a muscle twitch, isometric force was allowed to develop to a user-selected, constant, afterload. The controller then transitioned to isotonic mode, thereby allowing the muscle to shorten at that constant afterload until the muscle could no longer sustain the afterload. At this point, the controller transitioned to isometric mode to allow the muscle force to dissipate, whereupon the muscle was re-stretched to its initial length.

A detailed description of our Windkessel loading technique has been published previously (Garrett *et al.*, 2017; Garrett *et al.*, 2019). Briefly, a 3-element Windkessel transfer function (Z_{WK}) was used to model the flow impedance experienced by the left ventricle, dictated by the mechanics of the large arteries and peripheral arterial system. The impedance transfer function of the model is as follows:

$$Z_{Wk}(s) = \frac{(Z_C R_P C)s + (Z_C + R_P)}{(R_P C)s + 1}$$

The impedance is equivalent to an electrical low-pass filter containing two resistors and a capacitor. In this analogy, voltage and current are analogous to pressure and blood flow rate, respectively. The model was parameterised by the characteristic aortic impedance (Z_C, Pa·s·m^{-3}), the arterial compliance (C, m^3·Pa^{-1}) and the peripheral resistance (R_P, Pa·s·m^{-3}), the values of which were adapted from our previous study (Garrett *et al.*, 2019). For any ventricular pressure, this impedance transfer function was used to predict, in real-time, a corresponding ventricular outflow rate. The predicted outflow rate was then scaled using Laplace's Law, and used to control the rate of muscle shortening. Muscle re-stretch

rate was the same as that used for the conventional work-loop to provide consistency between protocols, where muscle length was returned to L_o at a modelled 'flow rate' into the 'ventricle', transformed to muscle length via Laplace's Law. The model, encoded in a combination of software and hardware, was computed at a rate of 20 kHz, and used to control muscle length throughout each twitch.

Experimental procedure

Animal handling and euthanasia were performed in accordance with a protocol approved by The University of Auckland's Animal Ethics committee (reference number 002006). Four male Wistar rats (10 weeks old, 250 g to 300 g) were used. Prior to euthanasia, each rat was injected with heparin (1000 IU kg^{-1}). Euthanasia was achieved via isoflurane (5 % in O_2) and cervical dislocation. The heart was excised and immediately plunged into a chilled Tyrode solution. The aorta was cannulated and the vasculature Langendorff-perfused with Tyrode solution at room temperature. The Tyrode perfusate contained 130 mM NaCl, 6 mM KCl, 1 $MgCl_2$, 0.5 mM NaH_2PO_4, 10 mM HEPES, 10 mM glucose with addition of 0.3 mM $CaCl_2$ and 20 mM 2,3-butanedione monoxime, and pH of 7.4 by using Tris.

The heart was opened along the septal boundary and trabeculae dissected from the left ventricle. A suitably-sized trabecula was mounted onto hooks and advanced into the measurement chamber of the calorimeter. Superfusate containing Tyrode solution and 1.5 mM $CaCl_2$ was supplied at a constant flow rate of 0.55 µL/s. Contraction of the trabecula was induced via electrical field stimulation at a rate of 2 Hz. When muscle force had reached steady state, the muscle was stretched gradually to reach the optimal length (L_o) to achieve maximal active force production. Muscle dimensions, including L_o and the major and minor diameters, were measured using a microscope graticule. These dimensions were utilised to inform the Windkessel model as well for post-experimental data processing. The entire work-loop calorimeter was enclosed in an insulated chamber to minimise thermal fluctuations and optical disturbances. The ambient temperature within the enclosure was maintained at 32 °C. The combination of the rate of flow of superfusate, the rate of contraction, and temperature ensured sufficient muscle oxygenation (Han *et al.*, 2011).

Experimental interventions

Each trabecula was presented with both the conventional 'flat-topped' work-loop and the Windkessel model-based work-loop protocols. In the conventional work-loop protocol, the trabecula contracted isometrically until the force reached a user-defined afterload. The length controller then allowed the muscle to shorten isotonically at constant afterload until the force was no longer sustainable by the muscle. Isometric relaxation commenced and force diminished, prior to the muscle being re-stretched to its initial length in time for the next twitch. In the Windkessel-loaded work-loop protocol, the afterload was defined by using a 3-element model of vascular impedance, encoded in LabVIEW Hardware and Software control architecture, to compute changes in trabecula length throughout each twitch. These then dictated the corresponding trabecula length, which was imposed by a linear voice-coil motor.

A series of Windkessel work-loops was performed by decrementing the peripheral resistance term in six steps from a 'high' impedance load (800 GPa.s.m^{-3}) to a 'low' impedance load (50 GPa.s m^{-3}), interspersed with isometric contractions. The muscle was allowed to reach steady state at each work-loop and isometric contraction intervention. Isometric contractions were performed at decrements of length in 5-6 steps until active force was no longer detectable in order to obtain the

isometric force-length relation. Muscle force and length were recorded throughout, simultaneous with muscle heat rate.

The recorded heat rate measured upon muscle contraction contained three components: active heat, change of basal heat, and electrical stimulus heat artefact. Hence, subsequent to the active contraction intervention, two additional interventions were required in order to accurately reveal the active heat output of the contracting muscle. Firstly, the electrical stimulation was halted to allow muscle quiescence. The resting trabecula was subjected to a series of length-change interventions to obtain data on the change of basal heat rate, which we have previously shown to be length- and velocity-dependent (Garrett *et al.*, 2020; Garrett *et al.*, 2021). These data were needed to compensate for the change of basal heat rate that occurs with a change of length, even the in absence of work production. Secondly, the heat artefact arising from electrical stimulation of the muscle was determined by measuring the heat signal in the measurement chamber with the mounting hooks in place, but in the absence of the muscle. The active heat rate was revealed during each afterloaded work-loop contraction by subtracting from the measured heat rate signal the change of basal heat rate and the stimulus heat artefact.

Experimental design and muscle geometry

In total, n = 6 trabeculae isolated from four rat hearts were studied. Three were presented with the flat-topped work-loop intervention prior to the Windkessel work-loop intervention, while the other three received the converse order. Trabeculae, on average, had a minor diameter of 353 µm ± 20 µm, a major diameter of 390 µm ± 20 µm, and L_o of 3.24 mm ± 0.11 mm, giving an average cross-sectional area of 0.109 mm^2 ± 0.0099 mm^2 and volume of 0.354 mm^3 ± 0.0357 mm^3.

Data processing

Force was converted to stress by division with mean muscle cross sectional area. Muscle length was expressed relative to its optimal value (L/L_o). Work output was computed as the integral of stress with respect to length throughout a twitch, equivalent to the area of the stress-length work-loop. The extent of muscle shortening was given by the width of the work-loop. To calculate muscle heat rate, the thermopile voltage was corrected for stimulus heat and changes in basal heat, as described above, and then divided by the product of the thermopile sensitivity (4000 V/W). Muscle heat per twitch was calculated by further division by the stimulus frequency (2 Hz). Mechanical efficiency was calculated as the ratio of work to the sum of work and active heat, where the denominator signifies the change of enthalpy.

Statistical Analyses

Data were plotted as functions of either the normalised end-systolic stress (with respect to isometric maxima), muscle length (relative to optimal length) or peripheral resistance (R_p). Data points were fitted using polynomial regression, and the regression lines were averaged within contraction type (flat-topped and Windkessel) using the Random Coefficient Model implemented in the SAS software package. Peak values of variables were averaged and superimposed on the averaged regression lines, presented as mean ± standard error. Significant differences between peak values of variables were tested between contraction type using the paired T-test, and declared when $p < 0.05$.

Results

We compared flat-topped (conventional) with Windkessel loading methods on cardiac muscle mechanoenergetics. For the conventional loading protocol, trabeculae were subjected to 6 different 'constant' afterloads. For Windkessel loading, a series of Windkessel work-loops was performed by altering the peripheral resistance term in the Windkessel transfer function model. Figure 1 shows a typical experimental record of simultaneous measurement of twitch stress production and rate of active heat output from a representative trabecula, experiencing Windkessel loading. Rate of muscle active heat production (i.e. power) was calculated from the thermopile signal after first correcting for stimulus heat and changes in basal heat rate. Electrical stimulation commenced and the trabecula contracted isometrically until steady state (ISO), at which point the contraction mode was switched to 'work-loop' at a high afterload (labelled 'AF1'). Isometric contractions were performed, interspersed with work-loops at different afterloads. Heat rate decreased with decreasing afterload from 'AF1' (R_p = 800 GPa.s.m^{-3}) to 'AF6' (R_p = 50 GPa.s.m^{-3}).

In Figure 2, parametric plots of the steady-state twitches and length change yielded stress-length work-loops. The Windkessel work-loops exemplified (Figure 2C) the effect of the dynamic nature of the model-based load. These 'curve-topped' loops each display a shortening trajectory that arises from the implementation of modelled loads while mimicking the effect of the ventricular-arterial coupling which arises *in vivo*. By comparison, the conventional work-loops were flat-topped, consequent to the constant-force loads (Figure 2F).

The difference in the work-loop profiles between the two types of loading was further exemplified when the flat-topped (red) and Windkessel-loaded (blue) loops were superimposed in Figure 3A. The end-systolic points of the work-loops were fitted by quadratic regression to obtain the work-loop end-systolic stress-length relations for both contraction modes (Figure 3B). In Figure 3C, the end-systolic stress-length relations averaged from six trabeculae were not different between the Windkessel and the conventional work-loop contractions.

Closer examination of the shortening dynamics during loops at lowest load, for the same muscle as shown in Figure 3, provides a striking comparison, as shown in Figure 4. Although they may occasionally occur coincidentally, work-loops with comparable shortening cannot be directly prescribed by the experimentalist, as the afterload in Windkessel-loading arises from the peripheral resistance term, and is not explicitly controlled. A coincidentally matched afterload is exemplified by the two work-loops shown in Figure 4A-C. Despite similar afterloads, the times at end-systole (annotated by triangles) were different, but the times at end-contraction (annotated by filled circles) were closer between the two loading methods (Figure 4A-B). Figure 4D displays both the time to end-systole and the time to end-contraction, plotted as functions of end-systolic length normalised to L_o for a representative muscle. On average across the six trabeculae, there was a significant difference in the time to end-systole ($p < 0.0001$) but with no difference in the time to end-contraction ($p = 0.612$) between the two loading types (Figure 4E). These results indicate that trabeculae under the Windkessel loading protocol shortened at a lower velocity of shortening than under the conventional loading protocol (Figure 5). The average peak velocity of shortening was 2.56 s^{-1} ± 0.14 s^{-1} under the conventional loading but was 1.56 s^{-1} ± 0.13 s^{-1} under the Windkessel loading (Figure 5B), representing a difference of 39.0 % ± 5.0 % (p = 0.00514).

The increased stress development during shortening of the Windkessel work-loops yielded a greater work output, corresponding to the area of each work-loop. This result is revealed when work output is plotted as a function of end-systolic stress in Figure 6A and B, where the peak value of work output was greater under the Windkessel work-loop contraction than under the conventional work-loop contraction (0.84 kJ/m^3 ± 0.09 kJ/m^3 versus 0.70 kJ/m^3 ± 0.1 kJ/m^3; p = 0.00422). Heat output and enthalpy output were not different between the two work-loop contraction protocols (Figure 6C and D). Consequently, mechanical efficiency, quantified as the ratio of work to enthalpy, was greater under the Windkessel work-loop contraction than under the conventional work-loop contractions (peak value 17.8 % ± 2.1 % versus 14.4 % ± 1.8 %; p = 0.0369; Figure 6F). The relative end-systolic stress at which peak work occurred (namely the optimal end-systolic stress) was significantly lower under the Windkessel protocol than under the conventional work-loop contraction protocols (Figure 6B). The optimal relative end-systolic stress for peak work was 0.50 ± 0.02 under the Windkessel and 0.55 ± 0.03 under the conventional work-loop protocols (p = 0.0281). However, peak mechanical efficiency occurred at the optimal end-systolic stress (Figure 6F) of 0.41 ± 0.02 versus 0.45 ± 0.03 (p = 0.0610). These data are summarised in Figure 7 and expressed as fold-change, where the peak work was 21.8 % ± 4.7 % greater and the peak mechanical efficiency was 25.2 % ± 8.4 % greater under the Windkessel than under the conventional work-loop contractions. Figure 7E and F show, respectively, the work at peak efficiency (0.810 kJ/m^3 ± 0.088 kJ/m^3 versus 0.664 kJ/m^3 ± 0.096 kJ/m^3; p = 0.00429), and the heat at peak efficiency (4.06 kJ/m^3 ± 0.60 kJ/m^3 versus 4.14 kJ/m^3 ± 0.51 kJ/m^3; p = 0.730), expressed as fold changes.

Figure 8 displays work, heat, enthalpy and mechanical efficiency as functions of peripheral resistance (R_p) for the Windkessel work-loop contractions. The optimal R_p for peak work and for peak mechanical efficiency were interpolated from the curves and, have magnitudes of 174 GPa.s/m^3 ± 25 GPa.s/m^3 and 74 GPa.s/m^3 ± 20 GPa.s/m^3, respectively.

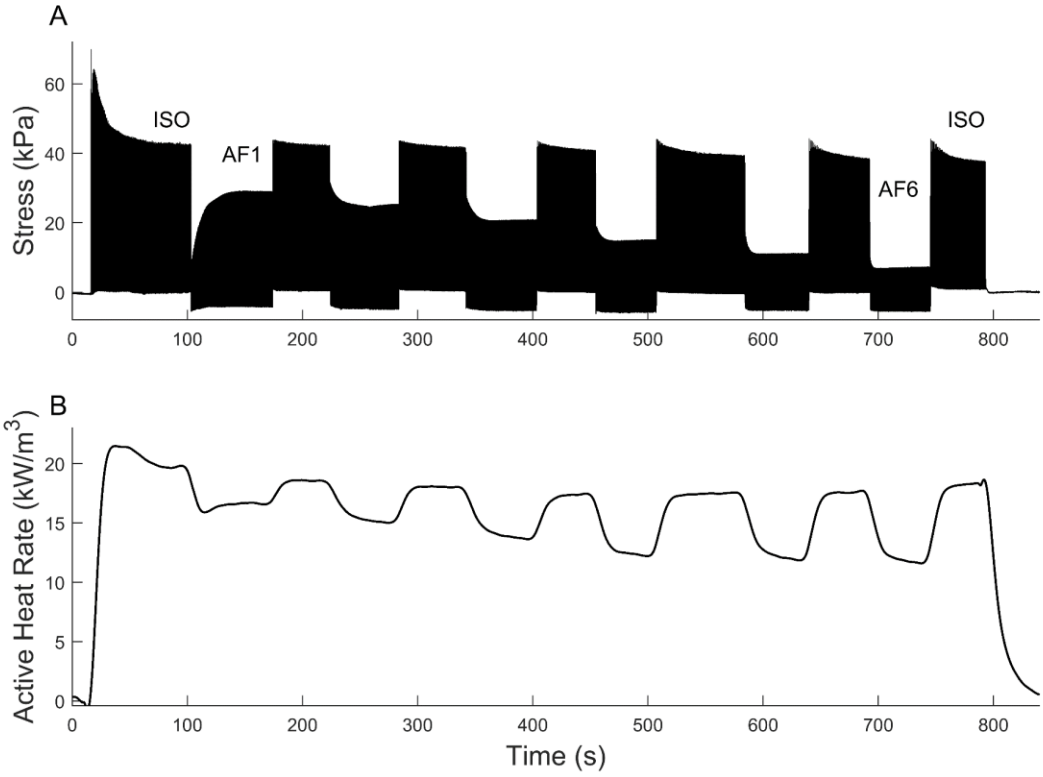

Figure 1: Simultaneous measurements of muscle stress and active heat rate. Data arose from a representative trabecula developing twitch stress (A) while liberating heat (B) upon 2-Hz electrical stimulation. Contraction mode alternated between isometric ('ISO') and Windkessel work-loop over six afterloads from a high impedance ('AF1', corresponding to a peripheral resistance of 800 GPa.s.m^{-3}) to a low impedance ('AF6', corresponding to a peripheral resistance of 50 GPa.s.m^{-3}). Within each contraction period, steady states of both twitch stress (A) and heat rate (B) were attained. A single twitch at steady state from each work-loop contraction period is shown in Figure 2A. Electrical stimulation was turned off at approximately 790 s and the muscle returned to quiescence.

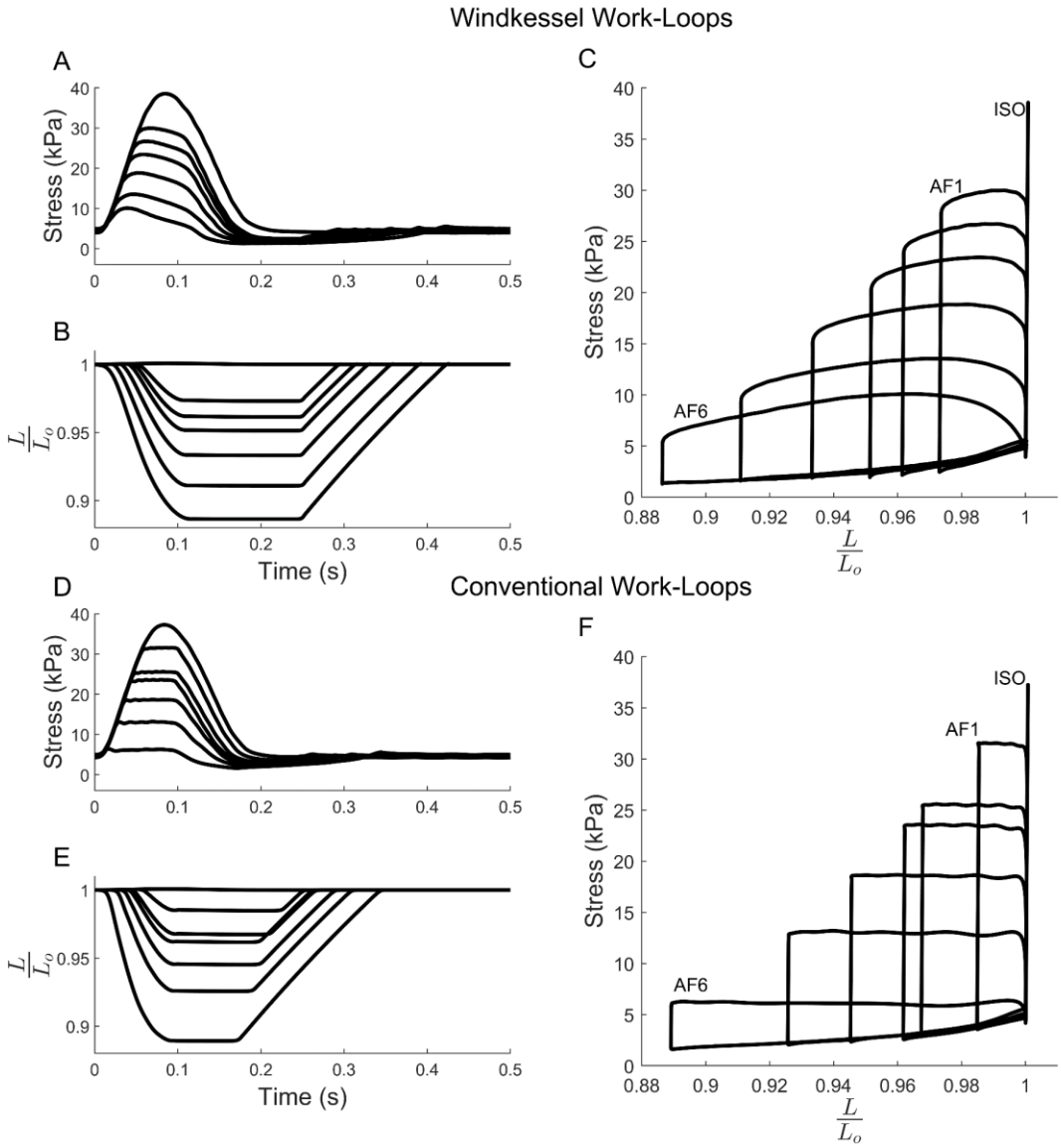

Figure 2: Comparison of Windkessel work-loops and conventional work-loops. Comparison is made from single steady-state, overlaid, twitches on the stress-time plane (A and D) and on the length-time plane (B and E), where the parametric plots reveal the stress-length work-loops (C and F). The Windkessel work-loops were achieved by changing the parameter governing the peripheral resistance, thereby varying the afterload. The labels 'ISO' (isometric), 'AF1' (high afterload) and 'AF6' (low afterload) are consistent with those in Figure 1. The conventional work-loops were achieved simply by setting different constant stresses (static afterloads). At all six afterloads, the Windkessel work-loops each had a shortening trajectory that was time-varying whereas the conventional work-loops maintained constant force throughout the shortening profile.

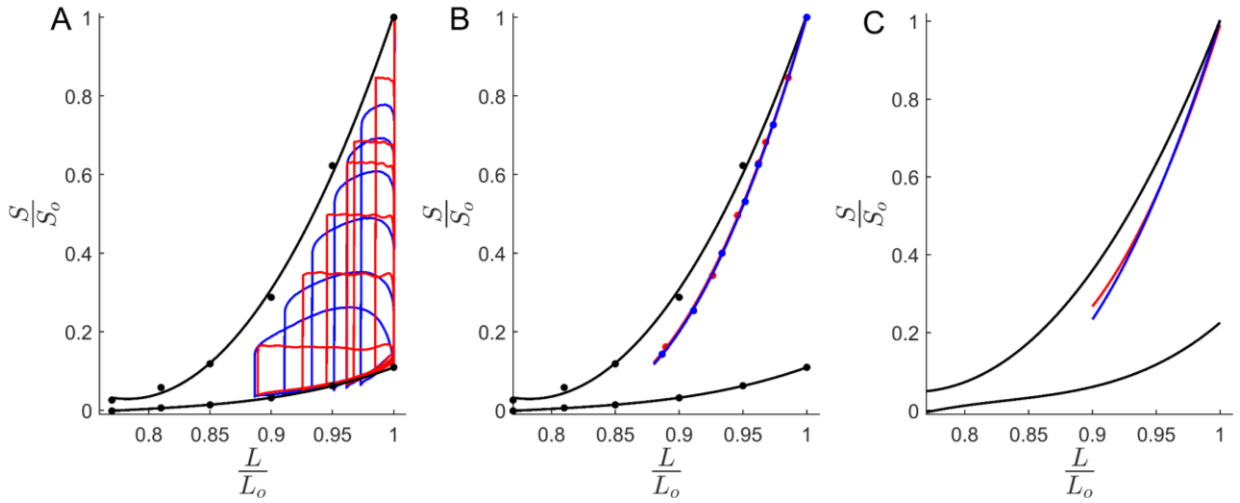

Figure 3: Mechanics of Windkessel work-loop (blue) and conventional (flat-topped) work-loop (red) contractions. Stress and length are normalised to the peak values at optimal length (L_o). Data in A and B have been plotted from the same trabecula as in Figure 2. The average regression lines from all 6 trabeculae are plotted in C. The stress-length work-loops in Panel A are the same data as in Figure 2C and 2F, but have been normalised to peak stress and superimposed to show differences between Windkessel loading (blue) and conventional loading (red). The black lines denote the isometric total stress-length relation (top) and the isometric passive stress-length relation (bottom), fitted to the data points using quadratic regression. Both isometric stress-length relations (black) in Panel A are reproduced in Panel B, along with the end-systolic points of the work-loop (red and blue points) which have also been fitted using quadratic regression. The regression lines were averaged across all 6 trabeculae and are plotted in Panel C, where no statistical difference was detected between the work-loop end-systolic relations arising from Windkessel loading and conventional loading.

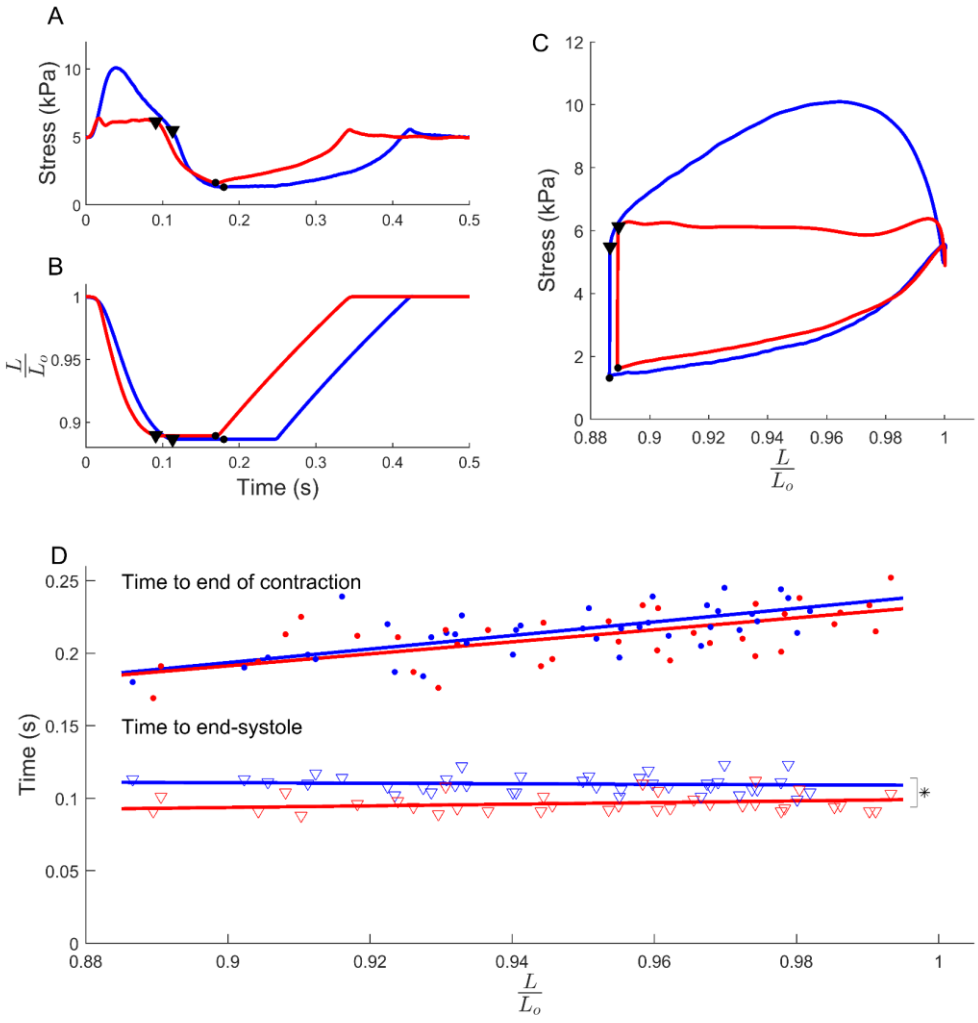

Figure 4: Time-course of muscle shortening during work-loop contractions. In Panels A-C, the data from the lowest afterload in Figure 2 between Windkessel (blue) and conventional (red) loading protocols are superimposed. The triangles indicate the time at end-systole (the end of muscle shortening), whereas the circles indicate the time to end of contraction when active stress production had ceased. Note that following isometric relaxation (at around 0.17 s; at the onset of the circles), the rate of muscle re-stretch was controlled to be the same for the two loading protocols. In Panel D, the two time-points (triangles and circles) were calculated for all afterloads and for six muscles, plotted as functions of relative end-systolic length (L/L_o) and fitted with linear regression. Statistical significance between the regression lines from Windkessel (blue) and conventional (red) loading type is indicated by the asterisk.

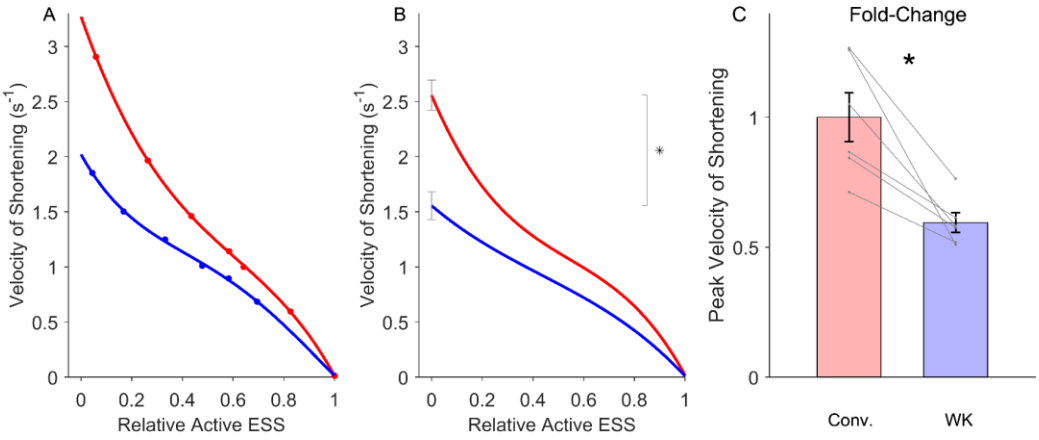

Figure 5: Velocity of shortening during Windkessel (blue) and conventional (red) work-loop contractions as functions of End-Systolic Stress. Data from a representative trabecula are shown in Panel A, and the average regression lines from all 6 trabeculae are plotted in Panel B. Velocity of shortening has been normalised to the optimal length (L_o) of trabeculae, and plotted against active end-systolic stress (ESS) relative to the optimal active stress at L_o. Velocity of shortening was computed from the twitch length profile (Figures 2B and 2E) as the maximal slope during the relaxation phase. Statistical significances between the peak velocity of shortening including the velocity-ESS regression lines from Windkessel (blue) and conventional (red) loading type is indicated by the asterisk. Panel C describes the fold-change for peak shortening velocity, displayed as means with standard errors normalised to the conventional loading (Conv.). Normalised peak velocity for each of the 6 trabeculae is paired between the two loading protocols (Conv: conventional; WK: Windkessel). The asterisk indicates a significantly lower peak velocity of shortening under the Windkessel loading in relation to that under the conventional loading.

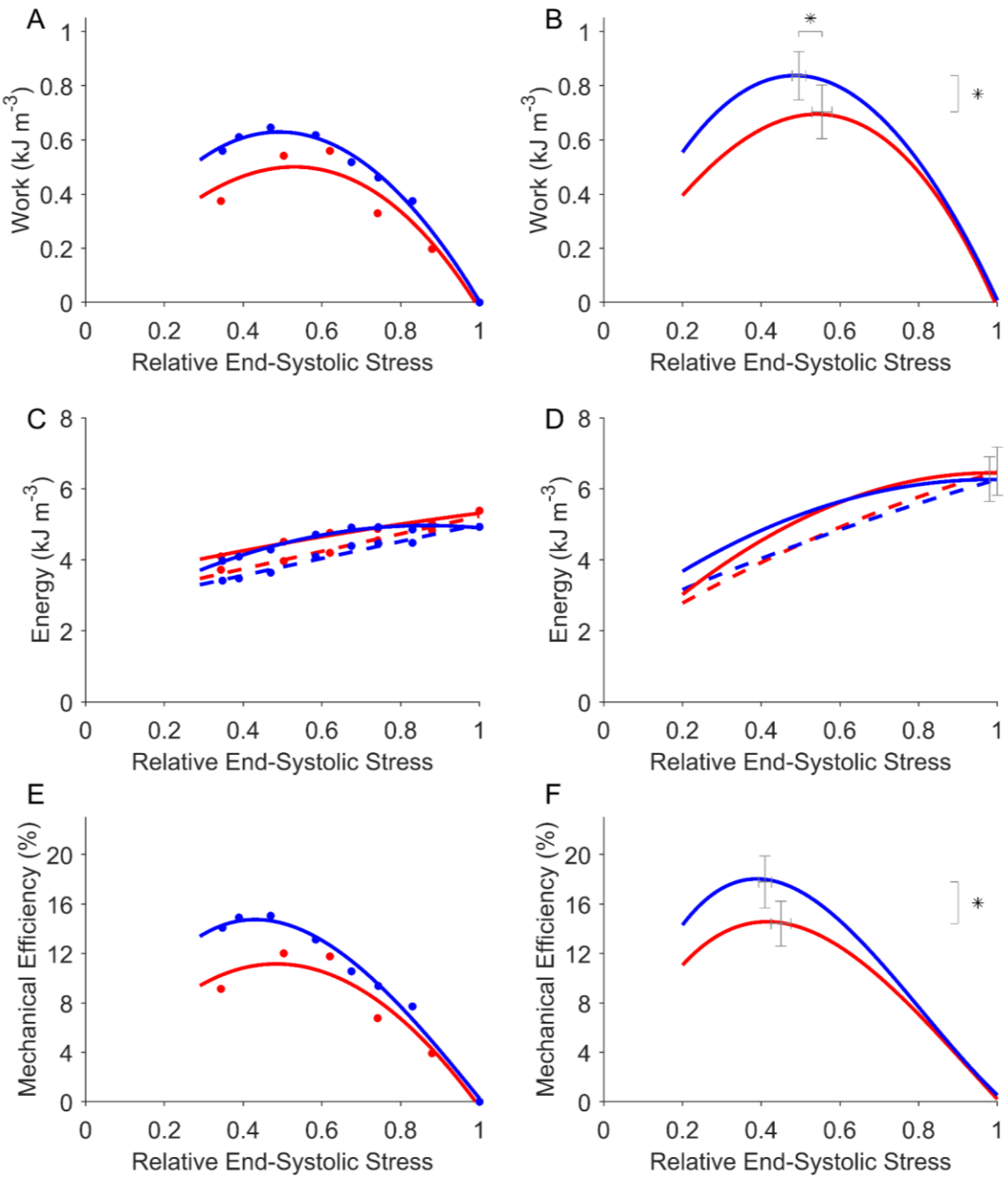

Figure 6: Mechanical efficiency of Windkessel (blue) and conventional (red) work-loop contractions. Data from a representative trabecula are shown in the left Panels (A, C and E), and the average regression lines from all 6 trabeculae are plotted in the right Panels (B, D and F). Work was quantified by integrating twitch stress with respect to length throughout the time course of each work-loop twitch, which denotes the area within each work-loop in Figure 3. Enthalpy is the sum of work and heat. Mechanical efficiency is the ratio of work to enthalpy. Data points are fitted using linear regression for heat (broken lines C and D), quadratic regression for enthalpy (solid lines in C and D), and cubic regression, constrained at the origin, for both work (A and B) and efficiency (E and F). All regression lines are drawn to commence at relative passive stress (0.2-0.3). End-systolic stress (ESS) was normalised to the peak stress obtained under isometric contractions at L_o. Standard errors of means are superimposed at peak values for each dependent variable. Statistical significance between Windkessel (blue) and

conventional (red) work-loop contractions are declared for both peak work (B) and peak mechanical efficiency (F), as indicated by the asterisks. The optimal end-systolic stress at which peak work occurred is significantly lower under the Windkessel than the conventional work-loop contractions (0.50 ± 0.02 versus 0.55 ± 0.03 relative end-systolic stress). However, the optimal end-systolic stress at which peak efficiency occurred is not significantly different between loading protocols (0.41 ± 0.02 versus 0.45 ± 0.03 relative end-systolic stress; $p = 0.0610$).

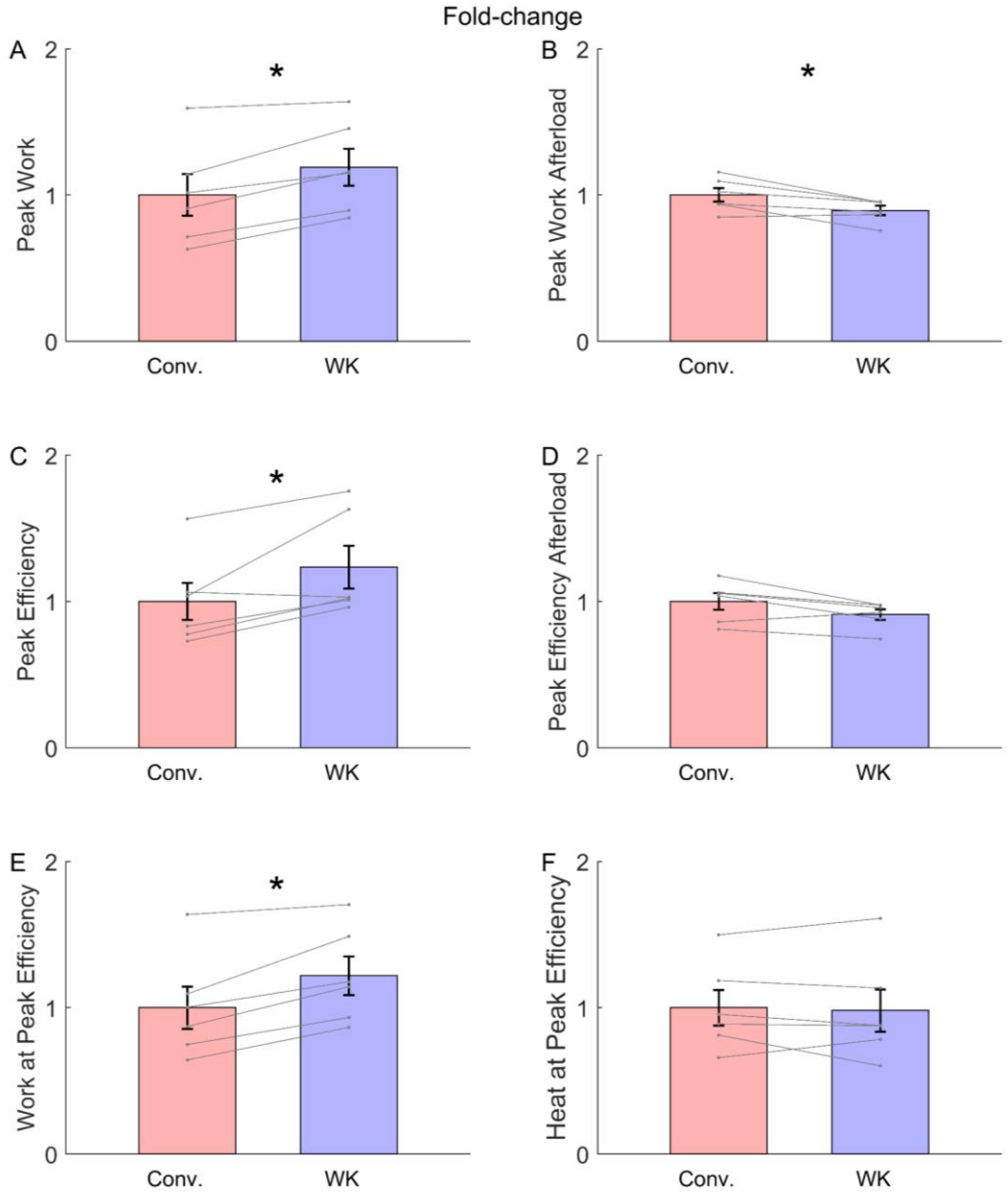

Figure 7: Fold-change of mechano-energetic indices from conventional loading to Windkessel loading. In all panels, mechano-energetic indices (calculated from Figure 6) from the Windkessel (WK) loading are normalised to those from the conventional (Conv.) loading. Data points are from all 6 muscles, each paired between the two loading types. Bars indicate means ± standard errors. Statistical significance between the two loading types is indicated by an asterisk. Panels A and C display the peak values for work and efficiency. Panels B and D show the optimal afterloads at which peak values for work and efficiency occur. Panels E and F show the work and the heat at the optimal afterload at which peak efficiency occurs. In panel D, p-value for the difference in fold change is 0.0610.

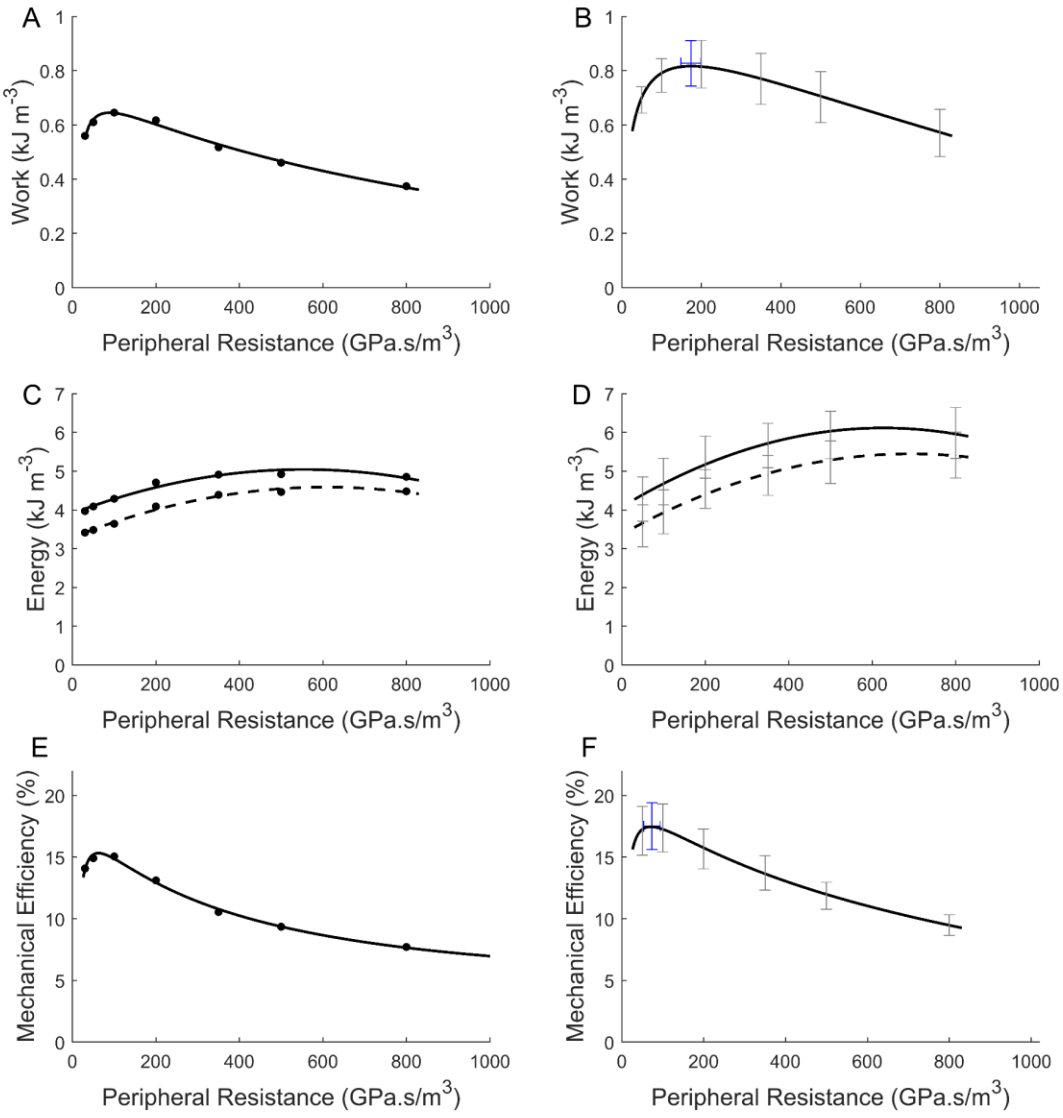

Figure 8: Energetics of Windkessel work-loop contractions as functions of peripheral resistance. Data from a representative trabecula are shown in the left panels (A, C and E), and the average regression lines from all 6 trabeculae are plotted in the right panels (B, D and F). Work, enthalpy, and mechanical efficiency (defined as in Figure 6) are displayed as functions of peripheral resistance (R_P). Each trabecula was subjected to the same range of peripheral resistance (R_p) and, hence, dependent variables (and their means and standard errors) can be plotted as functions of the independent variable, R_P. Data points are fitted using quadratic regression for enthalpy (C and D), using cubic regression for both work (A and B) and efficiency (E and F). The blue error bars in B and F are the interpolated peak values.

Discussion

In this study, we extend the use of the loading method based on a 3-element Windkessel model of the systemic arterial system to investigate cardiac mechanoenergetics in isolated trabeculae. By approximating, in real time, the arterial impedance experienced by the ventricle *in vivo*, an impedance load reflecting the haemodynamics of the arterial system is applied to cardiac muscle *in vitro*. This model-based loading allows, for the first time, for the evaluation of the effects of arterial haemodynamics on the mechanoenergetics of isolated trabeculae. Comparing the conventional and Windkessel loading methods, trabeculae *in vitro* liberated the same amount of active heat and underwent the same extent of shortening, over a wide range of afterloads prescribed by changing the model term governing peripheral resistance. However, with Windkessel loads, trabeculae developed greater stress during shortening, and shortened more slowly. Overall, with Windkessel loads, trabeculae accrued a 22 % increase in the peak work output, and, in consequence, contracted at a 25 % increase in peak mechanical efficiency.

Extension of previous Windkessel-loading protocols: Loading methods using 3-element Windkessel impedance loads have been previously reported in whole-heart experiments (Suga & Sagawa, 1977; Elzinga & Westerhof, 1980; Sunagawa *et al.*, 1982; Sunagawa *et al.*, 1983; Maughan *et al.*, 1984; Sunagawa *et al.*, 1985; Midei *et al.*, 1987; De Tombe *et al.*, 1993; Fukumitsu *et al.*, 2016) and in isolated tissue experiments (Elzinga & Westerhof, 1981, 1982; de Tombe & Little, 1994). However, the applied loads have been either fluid-air systems, or have been pre-calculated, utilising physical electronic circuits or computational simulation offline. Moreover, in some of the previous studies, the resulting contraction was applied only to a single twitch, and not until steady state of force production upon a change of loading condition is achieved. In comparison, our real-time computation application in this study imposes fully-parameterised and real-time-computed loads.

Selection of Windkessel parameters: In the comparison between loading methods, numeric values for the three Windkessel model parameters were selected in order to perform a comparable range of work-loops which spanned from afterloads in the vicinity of passive stress to afterloads approaching the isometric stress. Initial values for C (compliance), Z_c (characteristic impedance) and R_p (peripheral resistance) were adapted from our previous study where we have investigated the effects of each of the three model parameters, individually and the variation of all three in concert (Garrett *et al.*, 2019). As Z_c and C have much smaller effects on the magnitude of the impedance load, these two parameters were held constant in the current study (C = 32 $pm^3 \cdot Pa^{-1}$ and Z_c = 5 $GPa \cdot s \cdot m^{-3}$). Instead, varying R_p alone (from 50 $GPa \cdot s \cdot m^{-3}$ to 800 $GPa \cdot s \cdot m^{-3}$) resulted in a range of work-loops that spanned the range of the end-systolic force-length relation, allowing for comparison to the conventional loading method (Figure 2).

Windkessel loading increases efficiency: By applying a model-based loading method, we observed an average increase of 22 % in the peak work output. However, this increase in work was not accompanied by an increase in the heat output of the muscle, nor was the extent of shortening compromised in order to achieve the elevated work output. This indifference of heat on the dynamics of shortening indicates that, while the energy consumption of the contractile elements is dependent on load and extent of shortening, it is not dependent on the dynamics of the shortening achieved under these loads. The cross-bridges consume the same energy, liberate the same amount of heat, yet achieve more work. Protocol-independent heat output is not entirely surprising on two fronts. First, the two loading protocols result in the same total twitch duration where the time to full relaxation from the onset of

contraction is the same. Second, they result in the same end-systolic stress-length relation (Figure 3C) and the same heat-stress relation (Figure 6D). The increase of work output for the same heat output provides a 25 % increase in the mechanical efficiency. This increased mechanical efficiency to a peak value of 18 % is closer to that measured from the working-heart (after accounting appropriately for basal oxygen consumption) - 21 % (Han *et al.*, 2014). The lower efficiency arising during the conventional loading method implies that this protocol does not realise the full force-length work potential of the muscle, such that it is unnaturally constrained to operate at a lower efficiency. We discuss below that the greater efficiency from Windkessel loading reflects the higher force of shortening, which is achieved with a lower rate of shortening and affects the kinetics of relaxation.

Shortening characteristics: We evaluated muscle shortening during work-loop contractions using four distinct indices. The first index is the trajectory profile of shortening. As a consequence of the time-varying nature of the Windkessel model, muscle shortening occurs along a trajectory that produces work-loops with curved shortening profiles (Figure 2). These dynamic shortening profiles resemble the pressure-volume ejection profiles exhibited by the ventricle observed *in vivo* (Sunagawa *et al.*, 1985; De Tombe *et al.*, 1993), which is unlike the conventional loading method that constraints the shortening trajectory to constant loads ('flat-top'). The dynamic nature of the ejection curve *in vivo* arises from the mechanical coupling between the pressure-driving ventricle and the compliant arterial system downstream. The large proximal arteries, acting as a filter, smooth out large ventricular cyclic pressure oscillations, thereby providing a more steady pressure source for the downstream arterial system (Westerhof *et al.*, 2009). These ejection mechanics *in vivo* are replicated for isolated trabeculae under our Windkessel loading, as is evident in the resulting curved shortening trajectory.

The second index we used to characterise muscle shortening was its extent of shortening, taken as the width of each work-loop. Under the Windkessel loads, despite a dynamic, curved, shortening trajectory, the extent of shortening achieved is not different from that obtained under the conventional constant load. This reveals that the greater force developed during shortening under the Windkessel loading did not compromise the extent of shortening. This behaviour yields the same end-systolic stress-length relations (Figure 3). Note that the end-systolic stress-length relations from the two work-loop contractions are different from that obtained from the isometric contraction (Figure 3), which is consistent with the concept of cardiac contraction mode-dependency (Han *et al.*, 2019; Tran *et al.*, 2020), which holds that a work-loop contraction that causes muscle shortening has its end-systolic point located below that of the isometric contraction.

The curved shortening trajectory, along with the same extent of shortening achieved in the Windkessel work-loop contraction versus the conventional work-loop contraction, prompts us to evaluate the time to reach end-systole. This third index for characterising muscle shortening reveals that trabeculae under Windkessel loading took longer to reach end-systole than when under the conventional loading (Figure 4). This finding suggests that the trabeculae shorten at a lower rate under the Windkessel loading. We therefore characterise muscle shortening by quantifying the velocity of shortening, and find, unsurprisingly, that this fourth index is indeed lower under Windkessel loading (Figure 5).

What is surprising to us, however, is that muscles shortening against the Windkessel load exhibit a different velocity-stress relation. We are aware that a different, lower, velocity-stress relation can be obtained at a lowered preload (Strauer, 1973; Gulch & Jacob, 1975; Tran *et al.*, 2020), at a reduced inotropic state (Tran *et al.*, 2020), at a lower temperature (de Tombe & ter Keurs, 1990), or from

muscles of different ventricular origin (Brooks *et al.*, 1987; Pham *et al.*, 2017), or those that have a larger proportion of the beta isozyme comprising the myosin heavy chain (Brooks *et al.*, 1987; Han *et al.*, 2021). Our experimental conditions meet none of these criteria. We thus consider that it is solely the difference in the control schemes employed in the two loading protocols that allows the difference in the position of the velocity-stress relation. Our thinking is supported by a previous study (Gillebert *et al.*, 1989) following our detailed scrutiny of their experimental records. Although not explicitly quantified, their raw experimental data show a lower velocity of shortening immediately ensues upon an increase in load during the shortening phase of the work-loop twitch. Whereas they employed the conventional loading protocol, which resulted in flat-top work-loop, clamping of the load to increase the force at the early, medium, and late time-points during the shortening phase all resulted in a decrease in the gradient of the length-time traces, suggesting a decrease in the velocity of shortening. Hence, their results and ours demonstrate that different loadings during the shortening phase affect the velocity of muscle shortening.

Taking all these four indices together in characterising muscle shortening, we show that the Windkessel load, owing to its dynamic nature, results in trabeculae developing greater force, over and above the force achieved under conventional loading. Greater force is associated with muscle shortening at a lower rate, thereby spending more time during shortening and taking longer to reach end-systole. In comparison, the conventional 'flat-top' loading protocol, where muscle length is controlled to maintain a constant force of shortening, shortens the muscle rapidly, and restricts it from developing force as high as that achieved during the Windkessel loading.

Relaxation characteristics: An interesting characteristic was obtained during the relaxation phase of work-loop. The total time to relaxation from onset of contraction remains unchanged despite the two distinct loading protocols affecting the time to end-systole (Figure 4). Thus, the slower shortening phase induced by the Windkessel loading is followed by a faster isometric relaxation phase than for the conventional loading, resulting in no difference in the time to full relaxation from the onset of contraction. The faster isometric relaxation phase does not appear to be a consequence of the difference in the timing of re-stretch of the two loading schemes, where the conventional loading re-stretches muscle immediately after complete relaxation, whereas the Windkessel loading allows the muscle to remain at end-systolic length for a longer period of time (Figure 4B). Note that under each of the two loading protocols, the rate of muscle re-stretch, dictated by a constant filling flow rate to the 'ventricle' in the model, is the same for both loading protocols. In both cases, we have allowed the muscle to relax fully prior to re-stretching.

The faster relaxation under the Windkessel loading seems to be a consequence of the higher force development during shortening. We are aware of studies demonstrating that cardiac muscle relaxation is sensitive to load. In our experiments, each muscle underwent isometric relaxation, consistently between the two loading protocols. In contrast, isotonic relaxation can be achieved by fully re-lengthening muscle following end-systole, i.e., stretching of the muscle back to its initial length before complete relaxation. The resultant work-loop twitch has a prolonged 'flat-top' region given the re-lengthening to maintain the constant afterload following end-systole. This isotonic relaxation method directly modifies the relaxation pattern to demonstrate that a stretch is necessary to accelerate relaxation (Lecarpentier *et al.*, 1979; Brutsaert *et al.*, 1980; Goethals *et al.*, 1980; Brutsaert & Sys, 1988). Isotonic relaxation can also be achieved by re-stretching the muscle at variable rates following end-systole. Such isotonic relaxation also directly modifies the relaxation pattern and reveals that

myocardial relaxation is sensitive to strain rate (Chung *et al.*, 2017; Chung, 2019). The consistent finding from these isotonic relaxation methods is that a delayed end-systole accelerates relaxation. Our results, from isometric relaxation, are in agreement that the delayed end-systole under the Windkessel loading accelerates relaxation. These data illustrate the sensitivity of muscle relaxation to load, and support our assertion that the faster relaxation under the Windkessel loading accompanies higher force production during shortening.

A link to the whole-heart: By computing and applying a dynamic afterload based on a Windkessel model, parameterised by measureable biophysical properties of the arterial system and ventricular-arterial coupling, the effects of changing model parameters can now be explored. Here, we demonstrate the exploration of varying the peripheral resistance term (R_p) in the modelled load to perform a wide range of work loops, where the work and efficiency can now be expressed as functions of this model parameter (Figure 8). The resulting relationships exhibit a relatively sharp peak at low values of R_p, that decays with increasing R_p, aligning with those observed in whole-heart impedance loading experiments (Westerhof & Elzinga, 1978; Piene & Sund, 1979; Piene, 1984; van den Horn *et al.*, 1984; Sunagawa *et al.*, 1985; van den Horn *et al.*, 1985; Elzinga & Westerhof, 1991; De Tombe *et al.*, 1993). Plotting measured mechanoenergetic variables in the whole-heart studies have allowed understanding of the interaction and matching between the left ventricle and the arterial impedance load. Our experimental approach now allows *in vitro* investigation of the ways in which arterial impedance parameters affect muscle work output and efficiency, while bridging the gap between muscle and whole-heart experiments.

Conclusion

In conclusion, this study reveals that isolated trabeculae, when impeded by a load modelled on *in vivo* arterial haemodynamics, realise more of their stress-length work potential, with increased mechanical efficiency. By contrast, the conventional ‘flat-top’ work-loop protocol may have restricted the work produced by the muscle, therefore constraining the muscle to operate at a lower efficiency. The increased mechanical efficiency is achieved directly from the increased force during shortening at a lower velocity without a change in the extent of shortening and heat production.

References

Barclay CJ, Widen C & Mellors LJ. (2003). Initial mechanical efficiency of isolated cardiac muscle. *J Exp Biol* **206,** 2725-2732.

Brooks WW, Bing OH, Blaustein AS & Allen PD. (1987). Comparison of contractile state and myosin isozymes of rat right and left ventricular myocardium. *J Mol Cell Cardiol* **19,** 433-440.

Brutsaert DL, Housmans PR & Goethals MA. (1980). Dual control of relaxation. Its role in the ventricular function in the mammalian heart. *Circ Res* **47,** 637-652.

Brutsaert DL & Sys SU. (1988). Load Dependence of Relaxation. In *Diastolic Relaxation of the Heart: Basic Research and Current Applications for Clinical Cardiology*, ed. Grossman W & Lorell BH, pp. 83-96. Springer US, Boston, MA.

Chemla D, Lau EM, Papelier Y, Attal P & Herve P. (2015). Pulmonary vascular resistance and compliance relationship in pulmonary hypertension. *Eur Respir J* **46,** 1178-1189.

Chung CS. (2019). How myofilament strain and strain rate lead the dance of the cardiac cycle. *Arch Biochem Biophys* **664,** 62-67.

Chung CS, Hoopes CW & Campbell KS. (2017). Myocardial relaxation is accelerated by fast stretch, not reduced afterload. *J Mol Cell Cardiol* **103,** 65-73.

De Tombe PP, Jones S, Burkhoff D, Hunter WC & Kass DA. (1993). Ventricular stroke work and efficiency both remain nearly optimal despite altered vascular loading. *Am J Physiol* **264,** H1817-1824.

de Tombe PP & Little WC. (1994). Inotropic effects of ejection are myocardial properties. *Am J Physiol* **266,** H1202-1213.

de Tombe PP & ter Keurs HE. (1990). Force and velocity of sarcomere shortening in trabeculae from rat heart. Effects of temperature. *Circ Res* **66,** 1239-1254.

Elzinga G & Westerhof N. (1973). Pressure and flow generated by the left ventricle against different impedances. *Circ Res* **32,** 178-186.

Elzinga G & Westerhof N. (1980). Pump function of the feline left heart: changes with heart rate and its bearing on the energy balance. *Cardiovasc Res* **14,** 81-92.

Elzinga G & Westerhof N. (1981). "Pressure-volume" relations in isolated cat trabecula. *Circ Res* **49,** 388-394.

Elzinga G & Westerhof N. (1982). Isolated cat trabeculae in a simulated feline heart and arterial system. Contractile basis of cardiac pump function. *Circ Res* **51,** 430-438.

Elzinga G & Westerhof N. (1991). Matching between Ventricle and Arterial Load - an Evolutionary Process. *Circulation Research* **68,** 1495-1500.

Frank O. (1899). Die Grundform des arteriellen Pulses. *Z Biol-Munich* **37**.

Fukumitsu M, Kawada T, Shimizu S, Turner MJ, Uemura K & Sugimachi M. (2016). Development of a servo pump system for in vivo loading of pathological pulmonary artery impedance on the right ventricle of normal rats. *Am J Physiol Heart Circ Physiol* **310,** H973-983.

Garrett AS, Loiselle DS, Han J-C & Taberner AJ. (2020). Compensating for changes in heart muscle resting heat production in a microcalorimeter. In *2020 42nd Annual International Conference of the IEEE Engineering in Medicine & Biology Society (EMBC)*, pp. 2557-2560. IEEE.

Garrett AS, Loiselle DS, Han J & Taberner AJ. (2021). Heat production in quiescent cardiac muscle is length-, velocity-, and muscle-dependent: Implications for active heat measurement. *Exp Physiol*.

Garrett AS, Pham T, Loiselle D, Han JC & Taberner A. (2019). Mechanical loading of isolated cardiac muscle with a real-time computed Windkessel model of the vasculature impedance. *Physiol Rep* **7,** e14184.

Garrett AS, Pham T, Loiselle DS, June-Chiew H & Taberner AJ. (2017). Real-time model-based control of afterload for in vitro cardiac tissue experimentation. *Conf Proc IEEE Eng Med Biol Soc* **2017,** 1287-1290.

Gillebert TC, Sys SU & Brutsaert DL. (1989). Influence of loading patterns on peak length-tension relation and on relaxation in cardiac muscle. *J Am Coll Cardiol* **13,** 483-490.

Goethals MA, Housmans PR & Brutsaert DL. (1980). Load-dependence of physiologically relaxing cardiac muscle. *Eur Heart J* **Suppl A,** 81-87.

Goo S, Joshi P, Sands G, Gerneke D, Taberner A, Dollie Q, LeGrice I & Loiselle D. (2009). Trabeculae carneae as models of the ventricular walls: implications for the delivery of oxygen. *J Gen Physiol* **134,** 339-350.

615 Gulch RW & Jacob R. (1975). Length-tension diagram and force-velocity relations of mammalian cardiac
616 muscle under steady-state conditions. *Pflugers Arch* **355,** 331-346.

617
618 Han J-C, Tran K, Crossman DJ, Curl CL, Koutsifeli P, Neale JPH, Li X, Harrap SB, Taberner AJ, Delbridge
619 LMD, Loiselle DS & Mellor KM. (2021). Cardiac mechanical efficiency is preserved in primary
620 cardiac hypertrophy despite impaired mechanical function. *Journal of General Physiology* **153**.

621
622 Han JC, Goo S, Barrett CJ, Mellor KM, Taberner AJ & Loiselle DS. (2014). The afterload-dependent peak
623 efficiency of the isolated working rat heart is unaffected by streptozotocin-induced diabetes.
624 *Cardiovasc Diabetol* **13,** 4.

625
626 Han JC, Pham T, Taberner AJ, Loiselle DS & Tran K. (2019). Solving a century-old conundrum underlying
627 cardiac force-length relations. *Am J Physiol Heart Circ Physiol* **316,** H781-H793.

628
629 Han JC, Taberner AJ, Kirton RS, Nielsen PM, Archer R, Kim N & Loiselle DS. (2011). Radius-dependent
630 decline of performance in isolated cardiac muscle does not reflect inadequacy of diffusive
631 oxygen supply. *Am J Physiol Heart Circ Physiol* **300,** H1222-1236.

632
633 Han JC, Taberner AJ, Kirton RS, Nielsen PM, Smith NP & Loiselle DS. (2009). A unique
634 micromechanocalorimeter for simultaneous measurement of heat rate and force production of
635 cardiac trabeculae carneae. *J Appl Physiol (1985)* **107,** 946-951.

636
637 Han JC, Taberner AJ, Nielsen PM, Kirton RS, Ward ML & Loiselle DS. (2010). Energetics of stress
638 production in isolated cardiac trabeculae from the rat. *Am J Physiol Heart Circ Physiol* **299,**
639 H1382-1394.

640
641 Helmes M, Najafi A, Palmer BM, Breel E, Rijnveld N, Iannuzzi D & van der Velden J. (2016). Mimicking the
642 cardiac cycle in intact cardiomyocytes using diastolic and systolic force clamps; measuring power
643 output. *Cardiovasc Res* **111,** 66-73.

644
645 Hisano R & Cooper Gt. (1987). Correlation of force-length area with oxygen consumption in ferret
646 papillary muscle. *Circ Res* **61,** 318-328.

647
648 Iribe G, Helmes M & Kohl P. (2007). Force-length relations in isolated intact cardiomyocytes subjected to
649 dynamic changes in mechanical load. *Am J Physiol Heart Circ Physiol* **292,** H1487-1497.

650
651 Iribe G, Kaneko T, Yamaguchi Y & Naruse K. (2014). Load dependency in force-length relations in isolated
652 single cardiomyocytes. *Prog Biophys Mol Biol* **115,** 103-114.

653

Lankhaar JW, Westerhof N, Faes TJ, Marques KM, Marcus JT, Postmus PE & Vonk-Noordegraaf A. (2006). Quantification of right ventricular afterload in patients with and without pulmonary hypertension. *Am J Physiol Heart Circ Physiol* **291,** H1731-1737.

Layland J, Young IS & Altringham JD. (1995). The length dependence of work production in rat papillary muscles in vitro. *J Exp Biol* **198,** 2491-2499.

Lecarpentier YC, Chuck LH, Housmans PR, De Clerck NM & Brutsaert DL. (1979). Nature of load dependence of relaxation in cardiac muscle. *Am J Physiol* **237,** H455-460.

Maughan WL, Sunagawa K & Sagawa K. (1984). Effects of arterial input impedance on mean ventricular pressure-flow relation. *Am J Physiol* **247,** H978-983.

Mellors LJ & Barclay CJ. (2001). The energetics of rat papillary muscles undergoing realistic strain patterns. *J Exp Biol* **204,** 3765-3777.

Mellors LJ, Gibbs CL & Barclay CJ. (2001). Comparison of the efficiency of rat papillary muscles during afterloaded isotonic contractions and contractions with sinusoidal length changes. *J Exp Biol* **204,** 1765-1774.

Midei MG, Maughan WL, Oikawa RY, Kass DA & Sagawa K. (1987). Extracardiac pressure changes do not alter contractile function of the isolated left ventricle. *Ann Biomed Eng* **15,** 347-359.

Pham T, Han JC, Taberner A & Loiselle D. (2017). Do right-ventricular trabeculae gain energetic advantage from having a greater velocity of shortening? *J Physiol* **595,** 6477-6488.

Piene H. (1984). Impedance matching between ventricle and load. *Ann Biomed Eng* **12,** 191-207.

Piene H & Sund T. (1979). Flow and power output of right ventricle facing load with variable input impedance. *Am J Physiol* **237,** H125-130.

Sagawa K, Lie RK & Schaefer J. (1990). Translation of Otto Frank's paper "Die Grundform des Arteriellen Pulses" Zeitschrift fur Biologie 37: 483-526 (1899). *J Mol Cell Cardiol* **22,** 253-254.

Saouti N, Westerhof N, Postmus PE & Vonk-Noordegraaf A. (2010). The arterial load in pulmonary hypertension. *Eur Respir Rev* **19,** 197-203.

Sorhus V, Sys SU, Natans A, Demolder MJ & Angelsen BA. (2000). Controlled auxotonic twitch in papillary muscle: a new computer-based control approach. *Comput Biomed Res* **33,** 398-415.

Strauer BE. (1973). Force-velocity relations of isotonic relaxation in mammalian heart muscle. *Am J Physiol* **224,** 431-434.

Suga H & Sagawa K. (1977). End-diastolic and end-systolic ventricular volume clamper for isolated canine heart. *Am J Physiol* **233,** H718-722.

Sunagawa K, Burkhoff D, Lim KO & Sagawa K. (1982). Impedance loading servo pump system for excised canine ventricle. *Am J Physiol* **243,** H346-350.

Sunagawa K, Maughan WL, Burkhoff D & Sagawa K. (1983). Left ventricular interaction with arterial load studied in isolated canine ventricle. *Am J Physiol* **245,** H773-780.

Sunagawa K, Maughan WL & Sagawa K. (1985). Optimal arterial resistance for the maximal stroke work studied in isolated canine left ventricle. *Circ Res* **56,** 586-595.

Taberner AJ, Han JC, Kirton RS, Loiselle DS & Nielsen PM. (2010). Stress development, heat production and dynamic modulus of rat isolated cardiac trabeculae revealed in a flow-through micro-mechano-calorimeter. *Conf Proc IEEE Eng Med Biol Soc* **2010,** 1860-1863.

Taberner AJ, Han JC, Loiselle DS & Nielsen PM. (2011a). An innovative work-loop calorimeter for in vitro measurement of the mechanics and energetics of working cardiac trabeculae. *J Appl Physiol (1985)* **111,** 1798-1803.

Taberner AJ, Han JC, Loiselle DS & Nielsen PM. (2011b). A work-loop calorimeter for measuring the force-length-heat relationship of working excised cardiac muscle fibers. *Conf Proc IEEE Eng Med Biol Soc* **2011,** 1901-1904.

Taberner AJ, Hunter IW, Kirton RS, Nielsen PMF & Loiselle DS. (2005). Characterization of a flow-through microcalorimeter for measuring the heat production of cardiac trabeculae. *Rev Sci Instrum* **76**.

Tran K, Taberner AJ, Loiselle DS & Han JC. (2020). Energetics Equivalent of the Cardiac Force-Length End-Systolic Zone: Implications for Contractility and Economy of Contraction. *Frontiers in Physiology* **10**.

van den Horn GJ, Westerhof N & Elzinga G. (1984). Interaction of heart and arterial system. *Ann Biomed Eng* **12,** 151-162.

van den Horn GJ, Westerhof N & Elzinga G. (1985). Optimal power generation by the left ventricle. A study in the anesthetized open thorax cat. *Circ Res* **56,** 252-261.

Westerhof N, Bosman F, De Vries CJ & Noordergraaf A. (1969). Analog studies of the human systemic arterial tree. *J Biomech* **2,** 121-143.

Westerhof N & Elzinga G. (1978). The apparent source resistance of heart and muscle. *Ann Biomed Eng* **6,** 16-32.

Westerhof N, Lankhaar JW & Westerhof BE. (2009). The arterial Windkessel. *Med Biol Eng Comput* **47,** 131-141.

Competing interests

All authors declare that they have no competing interests.

Data availability statement

The experimental data contributing to this study can be made available by the corresponding author upon request.

Author Contributions

Experiments, data analysis and initial manuscript drafting performed by AG. All authors contributed to the study design, data interpretation and final drafting and approval of manuscript.

Funding

The work was supported by a Doctoral Scholarship from The University of Auckland (awarded to AG), a Marsden Fast-Start grant (UOA1504) from the Royal Society of New Zealand (awarded to J-CH), a Sir Charles Hercus Health Research Fellowship (20/011) from the Health Research Council of New Zealand (awarded to J-CH), and a James Cook Research Fellowship from the Royal Society of New Zealand (awarded to AT).

Acknowledgements

None.